Research Square

Preprints are preliminary reports that have not undergone peer review.
They should not be considered conclusive, used to inform clinical practice,
or referenced by the media as validated information.

Numerical Investigation of the Aerodynamic Response and Flow-Field Characteristics of a Loitering Munition under Heavy Rain

Jiankang Yong
Wenfeng Guo
16616071@qq.com

Ning Du
Dejian Zhang

Research Article

Keywords: Loitering munition, Heavy rain, Aerodynamic characteristics, Computational fluid dynamics

Posted Date: November 13th, 2026

DOI: https://doi.org/10.21203/rs.3.rs-11532055/v1

License: This work is licensed under a Creative Commons Attribution 4.0 International License.
Read Full License

Additional Declarations: No competing interests reported.

Type of the Paper (Original Paper.)

Numerical Investigation of the Aerodynamic Response and Flow-Field Characteristics of a Loitering Munition under Heavy Rain

Jiankang Yong [1], Wenfeng Guo [1,*], Ning Du [1,] and Dejian Zhang [1]

1 The School of Equipment Engineering Shenyang Ligong University Shenyang 110159, Liaoning China
2 Liaoshen Industrial Group Co., Ltd, Shenyang 110045; China
* Correspondence: 16616071@qq.com

Abstract: To investigate the variations in the aerodynamic characteristics of a loitering munition in a rainfall environment, this study employs computational fluid dynamics to numerically simulate the flow field under rain-free conditions and heavy rain conditions with a liquid water content of LWC = 30 g/m³, at a freestream velocity of 30 m/s and angles of attack ranging from 0° to 12°. The SST k-ω turbulence model is used for the continuous phase, while an Eulerian–Lagrangian method with two-way momentum coupling is used for the discrete phase to track raindrop trajectories; a random walk dispersion model is also incorporated to describe the effects of turbulence on raindrop dispersion. The results show that the wall film distribution is markedly nonuniform. The film height over the main regions of the munition body and wings is approximately 0.2–0.5 mm, with a maximum of 1.5 mm at the wing root. The film mass is greater in localized regions of the munition body (approximately 55 mg) and smaller on the wing surfaces (approximately 20 mg), and the regions of maximum film mass and maximum film height do not completely coincide. Compared with rain-free conditions, the lift coefficient under heavy rain conditions decreases to varying degrees at all angles of attack, whereas the differences in drag coefficient between the two conditions are relatively small. As the angle of attack increases, the lift-to-drag ratio generally first increases and then decreases. Within the range of angles of attack investigated in this study, the maximum lift coefficient occurs at an angle of attack of 2° under both conditions; the maximum lift-to-drag ratios under rain-free and heavy rain conditions are approximately 9.975 and 9.683, respectively, representing a reduction of approximately 2.9% under heavy rain conditions compared with rain-free conditions. Over the angle-of-attack range of 0°–8°, the lift-to-drag ratio is generally lower under heavy rain conditions; over the range of 9°–12°, the lift-to-drag ratios under the two conditions are relatively close. The difference in lift coefficient between the two conditions generally decreases as the angle of attack increases, but the local differences in pressure and shear stress do not exhibit a regular trend. The effect of rainfall on the lift coefficient exhibits a certain dependence on the angle of attack: it is more pronounced at low angles of attack and gradually weakens at high angles of attack. The liquid film increases the surface roughness, and the decrease in negative pressure on the upper wing surfaces causes changes in the aerodynamic performance of the loitering munition.

Keywords: Loitering munition; Heavy rain; Aerodynamic characteristics; Computational fluid dynamics

1 Introduction

As a new type of intelligent weapon that combines the reconnaissance and surveillance capabilities of unmanned aerial vehicles with the strike capabilities of precision-guided munitions, loitering munitions have become key operational nodes in modern combat systems. As battlefield environments become increasingly complex, weapons and equipment inevitably need to carry out combat missions under extreme weather conditions, such as heavy rain and heavy snowfall, during their service life, placing higher demands on the ability of weapon systems to adapt to all environmental conditions. Heavy rain conditions may disturb the flight stability and aerodynamic characteristics of loitering munitions, thereby affecting their combat effectiveness and mission completion. At present, the development qualification and proving-ground testing of loitering munitions are mostly conducted under standard meteorological conditions. The effects of adverse weather factors in actual combat environments have not been adequately assessed, and the associated research foundation remains relatively weak. Therefore, a systematic investigation of the aerodynamic characteristics of loitering munitions under heavy rain conditions is of considerable theoretical significance and engineering value for revealing the patterns of aerodynamic evolution under extreme meteorological conditions, improving their adaptability to complex environments, and supporting the optimization of aerodynamic configurations.

A number of studies on the aerodynamic characteristics of aircraft under heavy rain conditions have been conducted in China and abroad. As early as 1941, Rhode [1] concluded from wind tunnel tests that raindrop impacts on aircraft under heavy rain conditions would degrade their aerodynamic performance. Gaudy M. Bezos et al. [2] evaluated the effects of heavy rain on the aerodynamic performance of a typical commercial transport aircraft airfoil (NACA 64-210) in wind tunnel tests. The results showed that heavy rainfall had a significant effect on the aerodynamic performance of the transport airfoil, with a more pronounced effect on high-lift configurations. Terry Michael Gunderson [3] compared the performance degradation of different airfoil surfaces in a rainfall environment in a wind tunnel. The results showed that surface treatments affected the extent of rainfall-induced performance degradation; hydrophobic coatings exacerbated this degradation, with a 25% reduction in lift and a 12.5-fold increase in drag. Hansman and Craig [4] conducted rainfall tests on three airfoils, NACA 0012, NACA 64-210, and Wortmann FX67-K170, at low Reynolds numbers and found that rainfall-induced lift losses could reach 5%–25%. Among them, the Wortmann FX67-K170 airfoil, which was designed primarily for laminar flow, suffered the most severe loss, with a reduction in lift of up to 25%.

With the development of computational fluid dynamics, an increasing number of researchers have adopted two-phase flow methods to numerically simulate the effects of rainfall. Valentine et al. [5,6] proposed one-way and two-way Lagrangian particle tracking algorithms to simulate the impact and splashing of raindrop particles on airfoils and found that raindrop splashing was one of the causes of aerodynamic performance degradation. Hossein Fatahian [7] conducted numerical simulations of the NACA 0012 airfoil under four meteorological conditions: dry, rain, icing, and combined rain and icing. The results showed that both rainfall and icing reduced lift and increased drag, with icing having the more pronounced effect. M. Vijayakumar [8,9] used CFD++ to numerically investigate the effects of localized low-pressure regions and heavy rainfall environments on a MALE-UAV in cruise. The results showed that symmetric low pressure reduced both lift and drag, with small changes in rolling and yawing moments, whereas asymmetric low pressure caused significant abrupt changes in roll and yaw. Rainfall reduced the stall angle by 2°, increased drag by 40%–60%, and reduced lift. Zhenlong Wu [10] investigated the effects of heavy rain on the flight stability and controllability of the DHC-6 Twin Otter aircraft. The results showed that heavy rain reduced rudder and aileron effectiveness and decreased the steady-state responses of sideslip angle, yaw rate, and roll angle, thereby weakening the aircraft's control capability. Using CFD, Zhang Ruimin et al. [11] found that, at small angles of attack, the water film on the airfoil surface was the main cause of the reduction in lift coefficient and the slight increase in drag coefficient. Yuan Peijun [12] compared the effects of the wall film model and the wall impact model on the calculated aerodynamic characteristics. The results showed that both models reflected the general trend of decreasing lift and increasing drag. In terms of the underlying mechanism, however, the film model could simulate the promotion of boundary-layer separation by film accumulation, which exacerbated lift loss at high angles of attack, whereas the impact model considered only momentum exchange and could not represent film spreading and accumulation. This study provides a reference for model selection in numerical simulations of low-speed aircraft under heavy rain conditions.

In summary, the experimental and numerical studies conducted to date have covered different research objects, including two-dimensional airfoils and complete aircraft, and have clarified the changes in aerodynamic performance caused by rainfall and the associated influencing factors. Building on these studies, the present work takes a tandem-wing loitering munition as the research object and compares its aerodynamic characteristics under rain-free and heavy rain conditions at a freestream velocity of 30 m/s and angles of attack of 0°–12°. The analysis focuses on changes in lift coefficient, drag coefficient, and lift-to-drag ratio. Together with the changes in pressure distribution and wall shear stress at representative angles of attack, the correspondence between changes in the overall aerodynamic forces of the loitering munition and differences in the local flow field is examined.

2 Numerical Simulation Methods

2.1 Multiphase Flow Model

Heavy rain conditions essentially involve gas–liquid two-phase flow, which can be numerically simulated using an Eulerian–Eulerian model or an Eulerian–Lagrangian model. The Eulerian–Eulerian model solves a set of momentum and continuity equations for each phase and couples the phases through pressure and interphase exchange coefficients. The Eulerian–Lagrangian model, in contrast, divides the flow into a continuous phase and a discrete phase and is applicable when the volume fraction of the discrete phase is below 10%–12%. For the continuous phase, the SST k-ω turbulence model is used to solve the steady mean Navier–Stokes equations for mass and momentum to obtain the external flow field of the loitering munition. Raindrop particles are treated as the discrete phase and simulated using the Eulerian–Lagrangian model. The Lagrangian equation of motion for raindrops [13] can be expressed as follows:

$$\frac{dv_{pi}}{dt} = \beta(v_i - v_{pi}) + g_i\left(\frac{\rho_D - \rho}{\rho_D}\right) \quad (1)$$

$$\beta = \frac{18\mu}{\rho_D D_p^2}\frac{C_{Dd}Re_p}{24} \quad (2)$$

$$C_{Dd} = \frac{K_1}{Re_p} + \frac{K_2}{Re_p^2} + K_3 \quad (3)$$

$$Re_p = \frac{\rho D_p |v_i - v_{pi}|}{\mu} \quad (4)$$

where v_{pi} and v_i are the velocities of the discrete and continuous phases, respectively, in the i direction; $\beta(v_i - v_{pi})$ is the drag force per unit particle mass; C_{Dd} is the particle drag coefficient; Re_p is the particle Reynolds number; ρ_D and ρ are the densities of the discrete and continuous phases, respectively; and D_p is the diameter of the raindrop particles.

2.2 Random Walk Model

With two-way momentum coupling, raindrop particles are affected by turbulence after entering the continuous phase, resulting in particle dispersion. In this study, a random walk dispersion model is used to describe the effects of turbulence on raindrop dispersion, and an integral time scale T is introduced, expressed as follows:

$$T = \int_0^\infty \frac{u_p'(t)u_p'(t-\tau)}{\overline{u_p'^2}} d\tau \quad (5)$$

where T is the integral time scale, which is proportional to the particle dispersion velocity; $u_p'(t)$ is the particle velocity fluctuation at time t; $u_p'(t-\tau)$ is the particle velocity fluctuation at time $(t-\tau)$; and τ is the time lag.

2.3 Wall Film Model

At present, two main models are used to simulate the effects of raindrops on a wall: the wall impact model and the wall film model. The wall impact model considers only momentum exchange and cannot represent film spreading and accumulation, whereas the wall film model can simulate splashing, breakup, and heat transfer after raindrops impact the wall. Therefore, the wall film model is selected in this study.

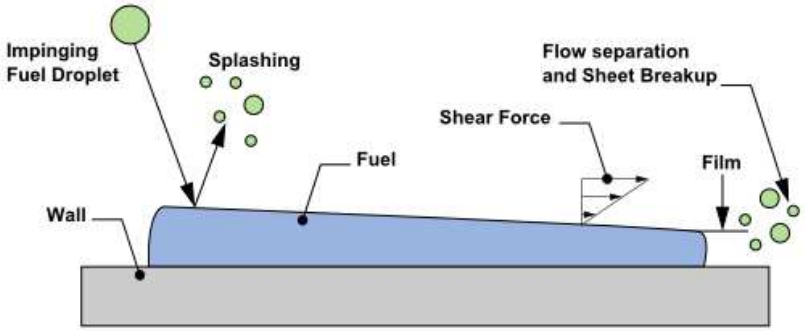


Fig. 1 Schematic illustration of the basic mechanisms of the wall film model

2.4 Simulation of Heavy Rain Conditions

Rainfall conditions can generally be described by parameters such as rainfall rate, liquid water content, raindrop diameter, and raindrop terminal velocity. Rainfall categories can be classified according to the accumulated rainfall over a specified period, as detailed in Table 1. Accumulated rainfall over a given period represents the total precipitation during that period, whereas rainfall rate represents the precipitation intensity per unit time; the two should not be compared directly. This study uses the instantaneous rainfall intensity and the corresponding liquid water content to describe the heavy rain conditions investigated.

Table 1 Classification of rainfall amounts over different periods

Category	Rainfall over the specified period (mm)	
	12 h rainfall	24 h rainfall

Trace rainfall	<0.1	<0.1
Light rain	0.1~4.9	0.1~9.9
Moderate rain	5.0~14.9	10.0~24.9
Heavy rain	15.0~29.9	25.0~49.9
Rainstorm	30.0~69.9	50.0~99.9
Severe rainstorm	70.0~139.9	100.0~249.
Extreme rainstorm	≥140.0	≥250.0

Two parameters, rainfall rate R and liquid water content LWC, are used in this study to describe the rainfall environment. The rainfall rate R represents the depth of the precipitation layer accumulated at the ground surface per unit time, in mm/h. The liquid water content LWC represents the mass of liquid water contained in a unit volume of air, in g/m³. The relationship between the two is described using the mathematical model proposed by Marshall in 1948:

$$LWC = 0.054R^{0.84} \quad \textbf{(6)}$$

The total raindrop mass flow rate Q represents the mass of raindrops passing through a specified cross-section per unit time and is calculated as follows:

$$Q = SV\square LWC \quad \textbf{(7)}$$

where Q is the mass flow rate, in kg/s; S is the rainfall area, in m²; and V is the freestream velocity, in m/s.

In numerical simulations, particle diameter distributions are mainly divided into two types: uniform and Rosin–Rammler distributions. For a uniform distribution, all particles released from the same injection source are assumed to have exactly the same initial diameter. A Rosin–Rammler distribution describes the particle size distribution using two parameters, the characteristic particle diameter and the spread parameter; a larger spread parameter indicates a more concentrated and more uniform particle size distribution. Under actual rainfall conditions, raindrop diameters span a certain range. To simplify the calculations, this study adopts an equal-diameter assumption, whereby raindrops released from the same injection source have the same initial diameter, and selects a representative diameter for a given rainfall intensity, calculated as follows:

$$D_p = aR^b\left(\frac{l-1}{l}\right)^{1/l} \quad \textbf{(8)}$$

where D_p is the particle diameter; a and b are empirical coefficients taken as 1.3 and 0.232, respectively; and l is the rainfall-type constant, taken as 2.25.

Raindrops are assumed to be spherical, nondeforming, nonevaporating, and noninteracting, with an initial velocity equal to the freestream velocity. During their fall, they are subjected only to gravity and aerodynamic drag. When aerodynamic drag and gravity are balanced, the raindrops reach their terminal velocity and fall at this constant velocity. This velocity can be calculated using the formula proposed by Markowitz [15]:

$$v_p = 9.58\left\{1-\exp\left[-\left(\frac{D_p}{1.77}\right)^{1.147}\right]\right\} \quad \textbf{(9)}$$

where v_p is the raindrop terminal velocity and D_p is the raindrop diameter.

The parameter settings for the heavy rain conditions investigated in this study are obtained from the above formulas for the raindrop parameters, as shown in Table 2.

Table 2 Rainfall parameters used in this study

R/(mm•h-1)	LWC/(g•m3)	D_p/mm	v_p/(m•s-1)
1848	30	5.758	9.352

3 Computations and Results

3.1 Grid Independence Verification

To ensure the reliability and accuracy of the numerical simulations, three grids with different resolutions, namely coarse, medium, and fine grids, were established for grid independence verification while maintaining $y^+ \approx 1$. Numerical simulations were conducted at a freestream velocity of 30 m/s to obtain the lift coefficients of the loitering munition at different grid resolutions, as shown in Table 3.

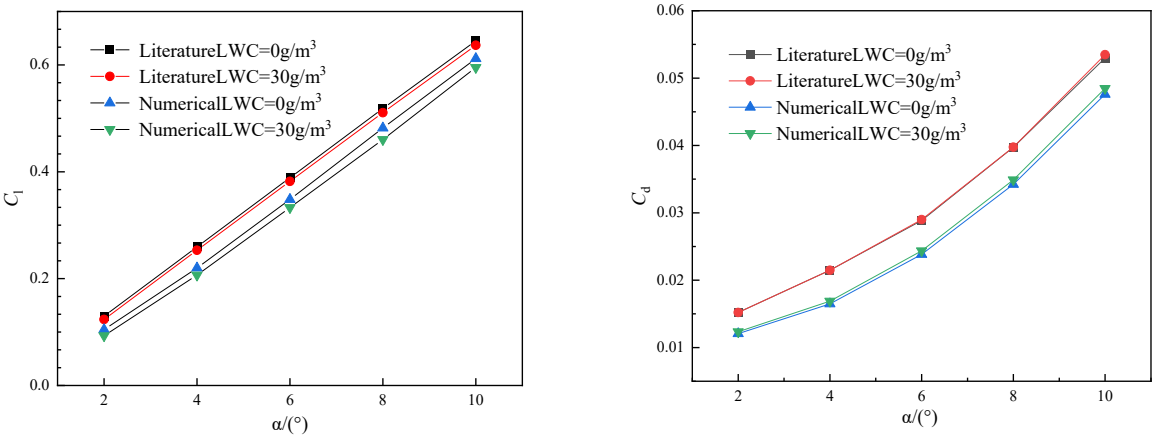
Table 3 Lift and drag coefficients at different grid counts

Grid resolution	Number of cells	Lift coefficient	Error relative to the fine grid	Drag coefficient	Error relative to the fine grid
Coarse grid	1311190	0.640	2.43%	0.0677	0.15%
Medium grid	3071097	0.652	0.61%	0.0663	1.92%
Fine grid	4959273	0.656	/	0.0676	/

As shown in Table 3, the error in the lift coefficient obtained with the medium grid relative to that obtained with the fine grid is only 0.61%, and the corresponding error in the drag coefficient is only 1.92%. Considering both computational accuracy and computation time, the medium grid is selected for the subsequent numerical simulations in this study.

3.2 Validation of Gas–Liquid Two-Phase Flow Coupling

To verify the accuracy and reliability of the numerical method adopted in this study for simulating the aerodynamic characteristics of a loitering munition under heavy rain conditions, numerical simulations were conducted using the NACA 0012 airfoil from Ref. [16], with a wing chord length of 1 m and a wingspan of 2 m. The SST k-ω turbulence model was used, and the Reynolds-averaged incompressible Navier–Stokes equations were solved using a pressure–velocity coupling algorithm. The SIMPLEC algorithm was selected to handle pressure–velocity coupling, and a second-order upwind scheme was used for pressure interpolation. The airfoil was specified as an adiabatic no-slip wall, the inlet was specified as a velocity inlet with a velocity of 30 m/s, and the outlet was specified as a pressure outlet. A raindrop diameter of 5.6 mm was selected to calculate the variations in the wing lift coefficient C_L and drag coefficient C_D at a liquid water content of LWC = 30 g/m³, and the numerical simulation results were compared with the values reported in the literature.



(a) Lift coefficient (b) Drag coefficient

Fig. 2 Comparison of lift and drag coefficients from the literature and the present study under heavy rain and rain-free conditions

As shown in Fig. 2, under both rain-free and heavy rain conditions, the lift coefficients calculated in this study are generally lower than the values reported in the literature, whereas the drag coefficients are generally higher. The trends with angle of attack are consistent, indicating that the present calculations can reproduce the basic trends in lift and drag coefficients in the reference case.

3.3 Model and Mesh Generation

This study investigates a tandem-wing loitering munition in which both the front and rear wings use the NACA 6409 airfoil. The munition consists of a body, front wings, rear wings, and tail surfaces, and all wings are rectangular. The body length is 1180 mm and the body diameter is 180 mm. The front and rear wingspans are 1600 mm and 1200 mm, respectively, and both have a chord length of 120 mm.

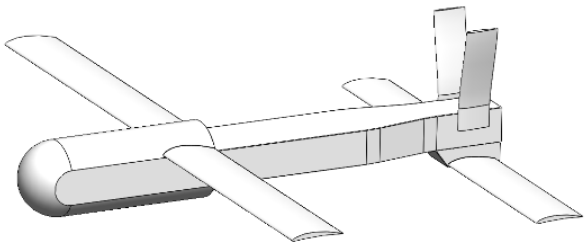


Fig. 3 Schematic of the loitering munition model

To effectively eliminate interference from the far-field boundaries with the flow field, the size of the external flow domain is set to ten times the characteristic length. Flow-domain meshes are divided into structured and unstructured meshes, and unstructured meshes are further divided into fully unstructured and hybrid meshes. A fully unstructured polyhedral mesh is adopted in this study, and the mesh around the munition body is refined to accurately capture flow-field variations near the wall. To facilitate mesh generation, fillets are introduced at the junctions between the wing roots and the munition body.

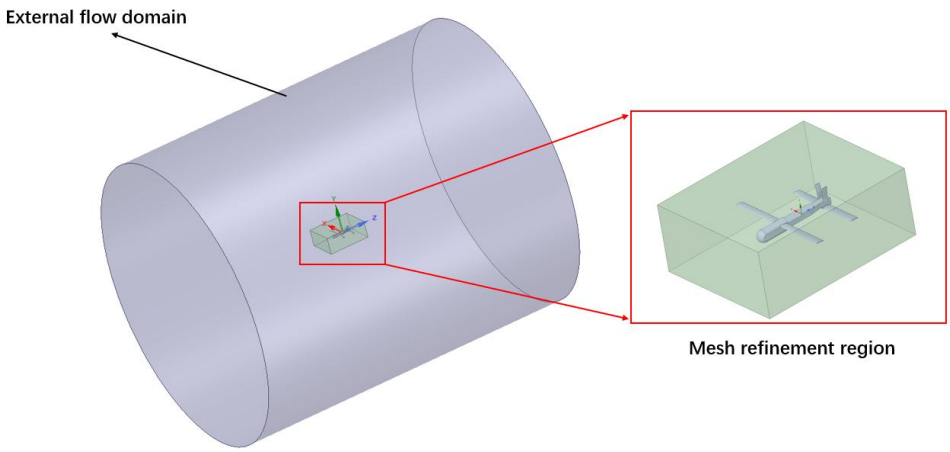


Fig. 4 Schematic of the computational domain partitioning

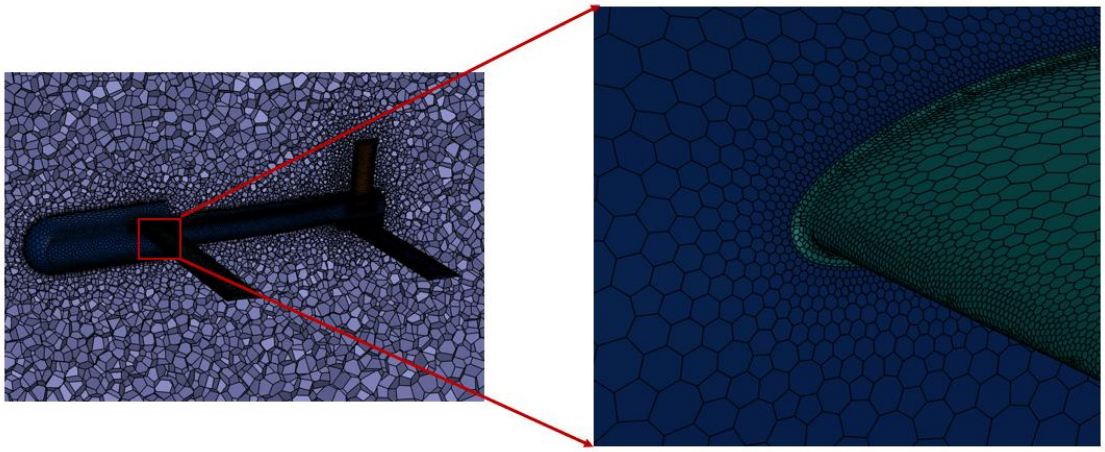


Fig. 5 Schematic of the mesh

3.4 Computational Results and Analysis

3.4.1 Liquid Film Distribution on the Loitering Munition Surface

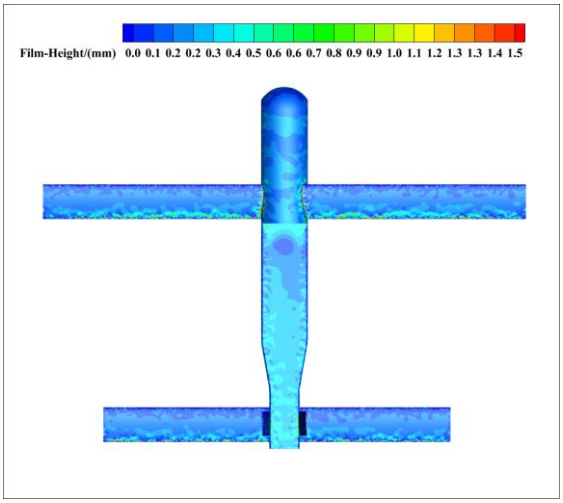


Fig. 6 Contours of liquid film height

As shown in Fig. 6, the liquid film height on the surface of the loitering munition is nonuniformly distributed. The film height over the main regions of the body and the front and rear wings ranges from 0.2 mm to 0.5 mm. Higher film

heights are mainly concentrated at the trailing edges of the wing surfaces, and the maximum occurs at the junction between the front wing and the body, where the film height reaches 1.5 mm. This is because the wall shear stress near the wing root is low and cannot effectively drive the film away from the wall, resulting in a significant reduction in the aerodynamic driving force acting on the film. Consequently, the film continues to accumulate and thicken under sustained rainfall.

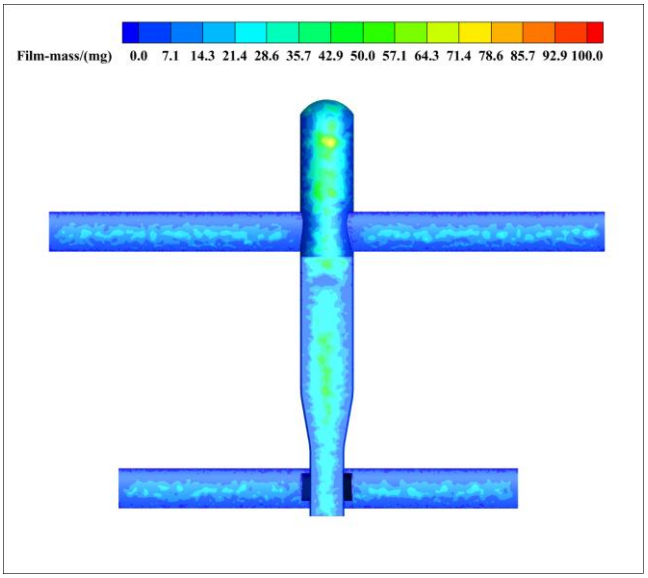


Fig. 7 Contours of liquid film mass

As shown in Fig. 7, the liquid film mass on the surface of the loitering munition is nonuniformly distributed. The film mass is relatively high near the body axis in the forward and middle-to-rear sections, at approximately 55 mg, whereas it is relatively low on the surfaces of the front and rear wings, at approximately 20 mg. The high-value regions on the body are distributed as localized patches and axial bands, while the higher-value regions on the wing surfaces extend intermittently in the spanwise direction. The overall distributions on the left and right wing surfaces are relatively similar, but the positions, sizes, and continuity of local patches differ to some extent.

In summary, the regions of maximum liquid film mass and maximum liquid film height do not completely coincide: the former are mainly located in localized regions of the munition body, whereas the latter are concentrated mainly at the wing trailing edges and wing–body junctions.

3.4.2 Lift and Drag Characteristics at Different Angles of Attack under Rain-Free and Heavy Rain Conditions

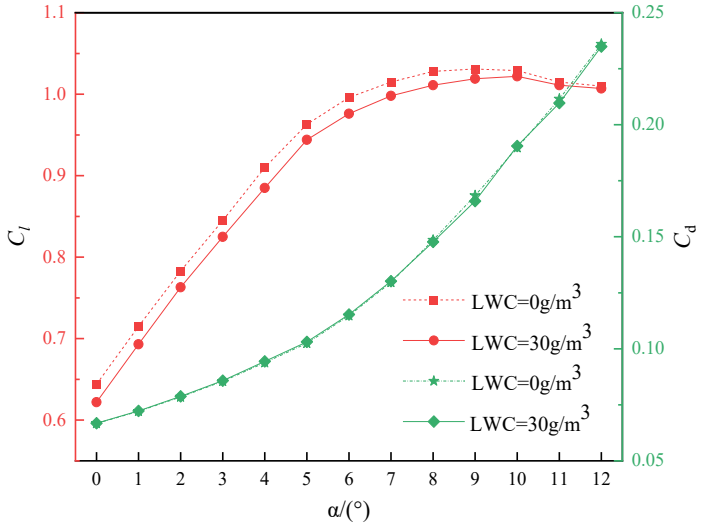


Fig. 8 Lift and drag coefficient curves

Figure 8 presents the variations in the lift and drag coefficients of the loitering munition with angle of attack under rain-free and heavy rain conditions. Over the angle-of-attack range of 0°–12°, the lift coefficient under both conditions

first increases relatively rapidly and then decreases slowly as the angle of attack increases, reaching its maximum at an angle of attack of 9° (1.031 under rain-free conditions and 1.019 under heavy rain conditions). Compared with rain-free conditions, the lift coefficient under heavy rain conditions is lower at every angle of attack. The differences are more pronounced at low and moderate angles of attack, whereas the two curves gradually approach each other at high angles of attack, indicating that the rainfall-induced lift loss generally decreases as the angle of attack increases. The overall trends of the lift curves under the two conditions are relatively consistent, indicating that heavy rain mainly reduces the lift level without significantly changing its basic variation with angle of attack. The drag coefficient increases continuously with angle of attack, and the increase becomes more pronounced beyond 9°. Compared with rain-free conditions, the change in drag coefficient under heavy rain conditions is small. The drag coefficients under the two conditions are relatively close, and their difference does not exhibit a consistent monotonic trend with angle of attack. Considered together with the changes in lift coefficient, the results show that while the increase in lift coefficient gradually slows and is followed by a slight decrease, the drag coefficient continues to increase. This indicates that the gain in lift obtained by increasing the angle of attack diminishes, while drag continues to increase.

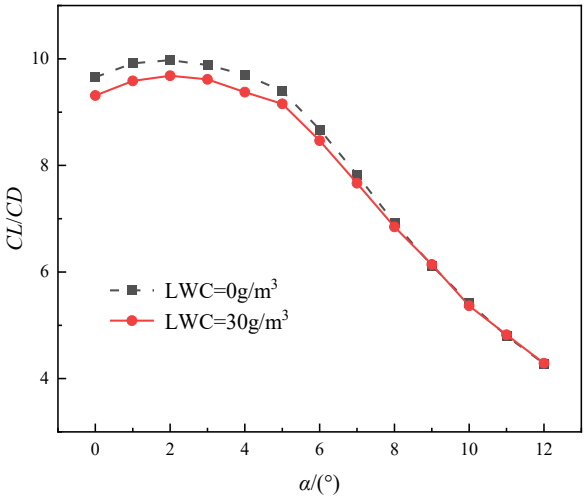
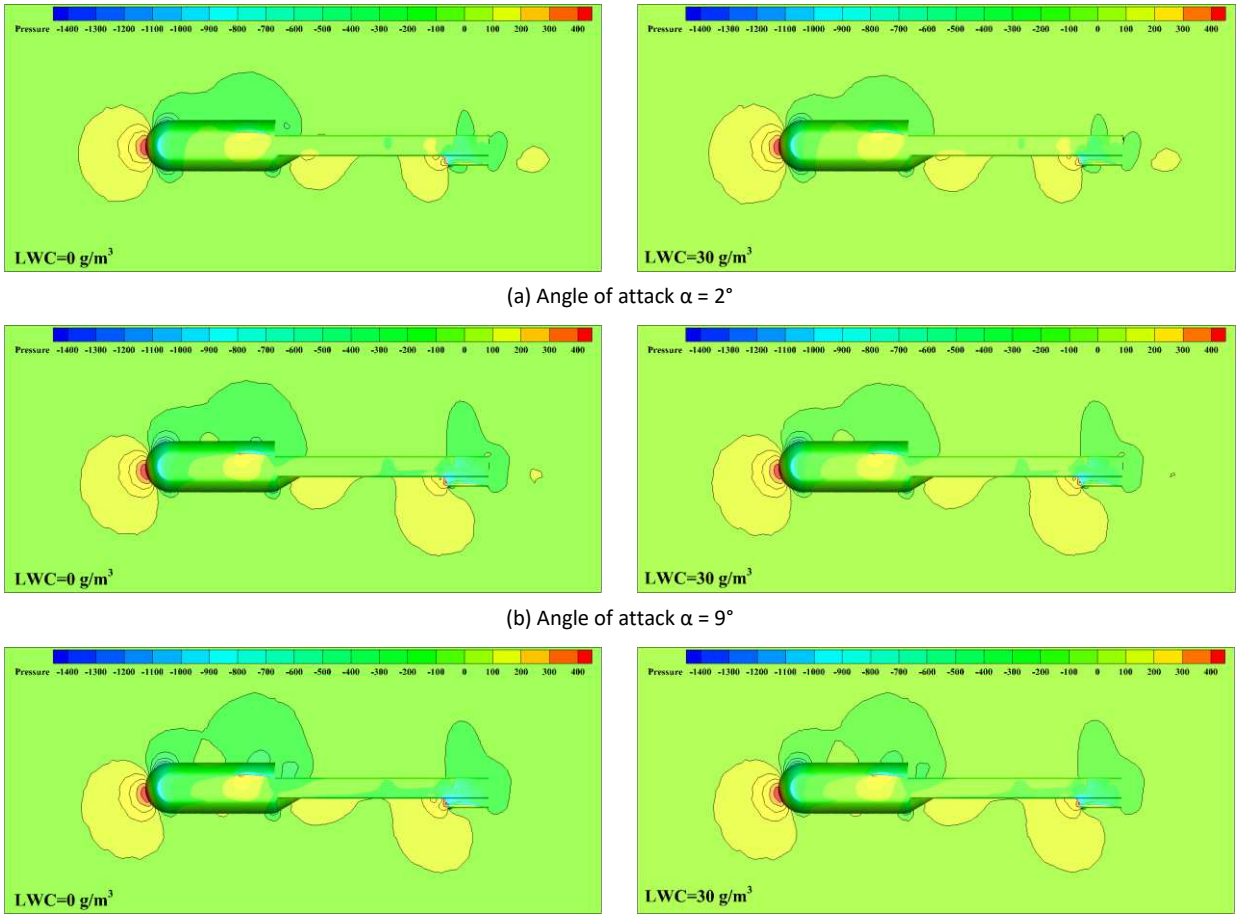


Fig. 9 Lift-to-drag ratio curves

Figure 9 presents the variations in the lift-to-drag ratio of the loitering munition with angle of attack under rain-free and heavy rain conditions. Over the angle-of-attack range of 0°–12°, the lift-to-drag ratio under both conditions first increases slightly and then decreases continuously, reaching its maximum at an angle of attack of 2°. The maximum lift-to-drag ratio is approximately 9.975 under rain-free conditions and approximately 9.683 under heavy rain conditions, representing a reduction of approximately 2.9%. This indicates that heavy rain reduces the maximum lift-to-drag ratio without significantly changing the corresponding angle of attack. Beyond an angle of attack of 2°, the lift-to-drag ratio gradually decreases, with a relatively rapid decline over the range of 5°–9°, and falls to approximately 4.28 at 12°. This indicates that the angle of attack corresponding to maximum lift is not the same as that corresponding to optimum aerodynamic efficiency. Considering the lift coefficient, drag coefficient, and lift-to-drag ratio curves together, the effects of rainfall on the aerodynamic characteristics of the loitering munition are manifested mainly as a reduction in lift, while its effect on drag is relatively weak. The lift loss also exhibits a certain dependence on the angle of attack, being more pronounced at low angles of attack and gradually weakening at high angles of attack.

3.4.3 Analysis of Flow-Field Characteristics at Representative Angles of Attack

Based on the above analysis of the lift coefficient, drag coefficient, and lift-to-drag ratio, three representative angles of attack, 2°, 9°, and 12°, are selected for a comparative analysis of the flow field on the longitudinal symmetry plane of the loitering munition under rain-free and heavy rain conditions. Figure 10 shows the pressure contours on the longitudinal symmetry plane of the loitering munition under rain-free and heavy rain conditions at angles of attack of 2°, 9°, and 12°.



(a) Angle of attack α = 2°

(b) Angle of attack α = 9°

(c) Angle of attack α = 12°

Fig. 10 Pressure contours on the longitudinal symmetry plane of the loitering munition

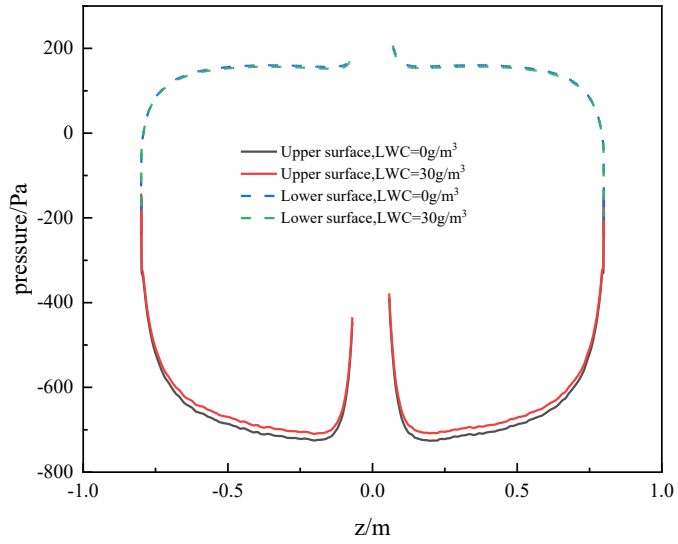
As shown in Fig. 10, at angles of attack of 2°, 9°, and 12°, the overall pressure distribution patterns on the longitudinal symmetry plane of the loitering munition are essentially consistent under rain-free and heavy rain conditions. Both exhibit localized high pressure at the windward end of the nose, low pressure above the forward body, and low pressure above and high pressure below the tail. As the angle of attack increases from 2° to 12°, the low-pressure region above the forward body generally expands upward. The high- and low-pressure regions around the tail expand more noticeably from 2° to 9°, whereas their overall extents change relatively little from 9° to 12°. This trend is observed under both conditions.

At the same angle of attack, the differences in pressure distribution caused by rainfall are relatively small. At an angle of attack of 2°, compared with rain-free conditions, the outer boundary of the positive-pressure region ahead of the nose expands slightly under heavy rain conditions, while the boundaries of the low-pressure regions above the forward body and the tail move slightly closer to the body. At an angle of attack of 9°, the main pressure regions under the two conditions remain relatively similar; only the upper boundary of the low-pressure region above the forward body is slightly lower, and the isolated positive-pressure patch downstream of the tail is noticeably smaller. At an angle of attack of 12°, the extents of the high-pressure region at the nose, the low-pressure region above the forward body, and the pressure regions around the tail are essentially the same. The pressure contours on the longitudinal symmetry plane of the loitering munition vary relatively noticeably with angle of attack, whereas rainfall mainly affects local pressure boundaries and contour shapes and has no pronounced effect on the pressure distribution.

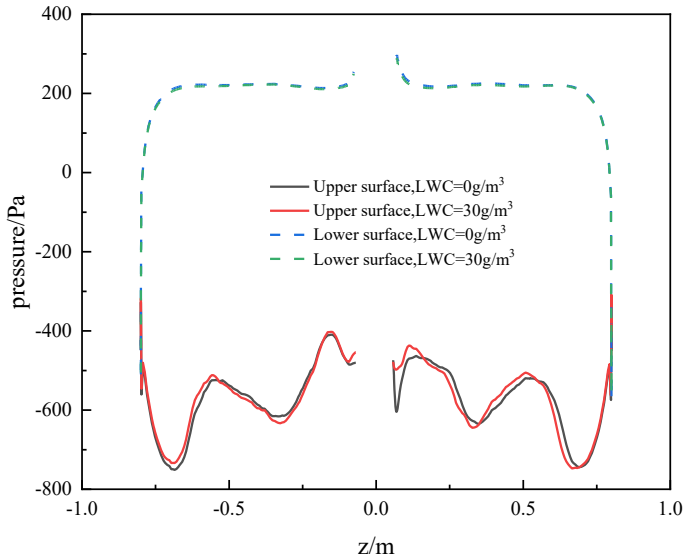
3.4.4 Analysis of Flow-Field Characteristics at a Wing Section at Representative Angles of Attack

The lift of aircraft with large wingspans is provided mainly by the wings. To investigate the effects of rainfall on the aerodynamic characteristics of the loitering munition, it is necessary to analyze the pressure distribution on the wing surfaces under rain-free and heavy rain conditions. In this study, the wing surface at a location 0.03 m from the wing leading edge is selected for analysis.

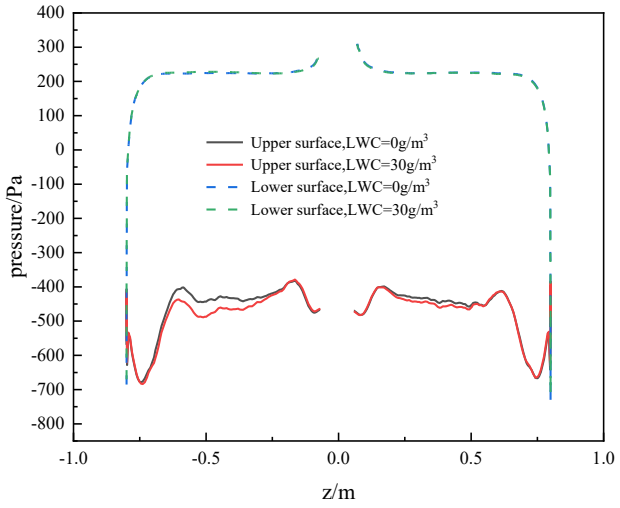
To further compare the local surface characteristics under the two conditions, a section 0.03 m from the leading edge of the front wing is selected, and the spanwise distributions of pressure and wall shear stress on its upper and lower surfaces are analyzed. The results are shown in Figs. 11 and 12, respectively.



(a) Angle of attack α = 2°



(b) Angle of attack α = 9°



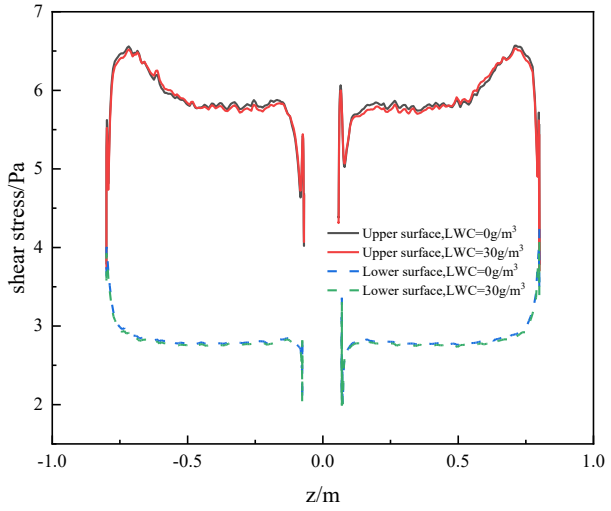
(c) Angle of attack α = 12°

Fig. 11 Wing surface pressure distribution curves

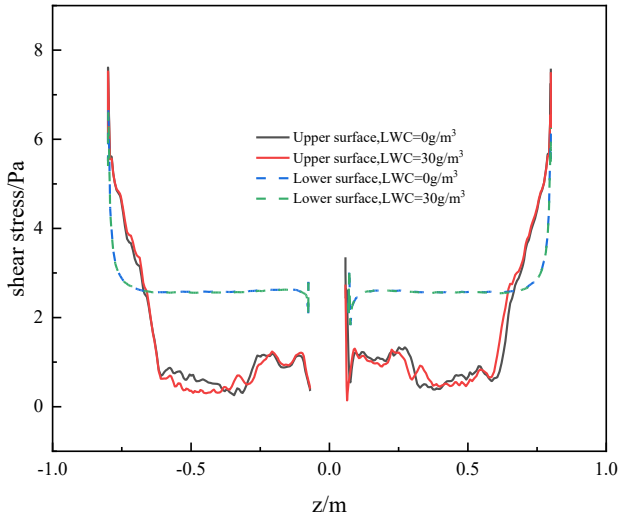
As shown in Fig. 11, at the section investigated, the overall pressure distribution patterns under rain-free and heavy rain conditions are similar. The differences between the two conditions occur mainly on the upper surface, while the pressure curves over the main spanwise region of the lower surface are relatively close.

At an angle of attack of 2°, the upper-surface pressure is generally slightly higher under heavy rain conditions than under rain-free conditions, meaning that the absolute magnitude of the negative pressure is reduced. At an angle of attack of 9°, the upper-surface pressure exhibits relatively pronounced spanwise fluctuations. The curves for the two conditions deviate from each other at some locations, and the direction of the pressure change varies with spanwise position. At an angle of attack of 12°, the fluctuations of the upper-surface pressure curve over the main spanwise region are weaker than at 9°, while local suction peaks remain near the wing tips. The pressure distributions under the two conditions are generally close, although differences can still be observed in some regions.

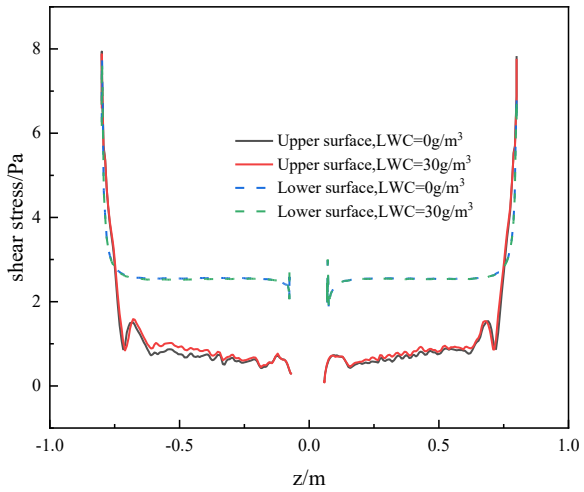
As the angle of attack increases, the pressure distribution at the wing section gradually changes from a relatively uniform spanwise distribution at low angles of attack to a more pronounced local redistribution of loading at moderate and high angles of attack. The additional effects caused by rainfall are characterized by an overall weakening of suction at low angles of attack, enhanced local pressure redistribution near 9°, and a weaker overall effect at 12°.



(a) Angle of attack α = 2°



(b) Angle of attack α = 9°



(c) Angle of attack α = 12°

Fig. 12 Wing surface shear stress distribution curves

As shown in Fig. 12, at an angle of attack of 2°, the shear stress on the upper surface is generally higher than that on the lower surface, with local peaks near the wing tips and a marked reduction near the wing roots. The upper-surface curves under the two conditions are generally close, with slightly lower values under heavy rain conditions, while the differences between the lower-surface curves are small. At an angle of attack of 9°, the differences in shear stress at some spanwise locations on the upper surface are more pronounced than at 2°. In particular, in the regions of low shear stress, the local peaks and troughs differ between the two conditions, and the direction of change varies with position. At an angle of attack of 12°, the shear stress over the main spanwise region of the upper surface is relatively low, with local peaks near the wing tips. The curves under the two conditions are generally close, although differences remain in some regions. At all three angles of attack, rainfall-induced differences in shear stress occur mainly on the upper surface, while the lower-surface curves are generally close.

4 Conclusions

This study numerically compares the aerodynamic characteristics of a loitering munition under rain-free (LWC = 0 g/m³) and heavy rain (LWC = 30 g/m³) conditions over an angle-of-attack range of 0°–12°. Together with the pressure contours on the longitudinal symmetry plane, the wing surface pressure distributions, and the wing surface shear stress distributions at representative angles of attack, the following conclusions are obtained:

(1) Rainfall has a relatively large effect on the lift coefficient, and this effect exhibits a certain dependence on the angle of attack. It is more pronounced at low angles of attack and gradually weakens at high angles of attack. Its effect on drag is relatively weak.

(2) Because the wall shear stress at the wing roots is low, it cannot effectively drive the liquid film away from the wall, causing the film to accumulate at the wing roots. Meanwhile, the liquid film on the surface of the loitering munition is nonuniformly distributed, and the regions of maximum film mass and maximum film height do not completely coincide.

(3) Under heavy rain conditions, the surface roughness of the loitering munition changes, leading to an increase in shear stress on the upper wing surfaces and a decrease in negative pressure on the upper surfaces, thereby causing changes in the aerodynamic performance of the loitering munition.

Funding： This study was funded by the Liaoning Talent Revitalization Program (No. XLYC2503071) and the National Natural Science Foundation of China (No. 12202285).

Declarations

- The authors have no relevant financial or non-financial interests to disclose.
- The authors have no competing interests to declare that are relevant to the content of this article.
- All authors certify that they have no affiliations with or involvement in any organization or entity with any financial interest or non-financial interest in the subject matter or materials discussed in this manuscript.
- The authors have no financial or proprietary interests in any material discussed in this article.

References

316 [1] Rhode RV (1941) Some effects of rainfall on flight of airplanes and on instrument indications. National Advisory Com
317 mittee for Aeronautics, Washington, D.C. NACA-TN-803
318 [2] Bezos GM, Dunham RE, Gentry GL et al (1992) Wind tunnel aerodynamic characteristics of a transport-type airfoil in
319 a simulated heavy rain environment. NASA, Washington, D.C. NASA-TM-107600
320 [3] Gunderson TM (2005) Study of the droplet surface interaction effects on a naturally laminar flow airfoil in multi-phas
321 e flow. Dissertation, University of Alberta, Edmonton. https://doi.org/10.7939/r3-z0v0-n308
322 [4] Hansman RJ, Craig AP (1987) Low Reynolds number tests of NACA 64-210, NACA 0012, and Wortmann FX67-K170 air
323 foils in rain. Journal of Aircraft 24:559-566. https://doi.org/10.2514/3.45476
324 [5] Valentine JR, Decker RA (1995) Tracking of raindrops in flow over an airfoil. Journal of Aircraft 32:100-105. https://do
325 i.org/10.2514/3.46689
326 [6] Valentine JR, Decker RA (1995) A Lagrangian-Eulerian scheme for flow around an airfoil in rain. International Journal
327 of Multiphase Flow 21:639-648. https://doi.org/10.1016/0301-9322(95)00007-K
328 [7] Fatahian H, Salarian H, Eshagh Nimvari M et al (2020) Effect of Gurney flap on flow separation and aerodynamic perf
329 ormance of an airfoil under rain and icing conditions. Acta Mechanica Sinica 36:659-677. https://doi.org/10.1007/s1040
330 9-020-00938-3
331 [8] Vijayakumar M, Parammasivam KM, Rajagopal S et al (2023) Effect of localised pressure depression and rain on aero
332 dynamic characteristics of MALE UAV. Defence Science Journal 73:385-393. https://doi.org/10.14429/dsj.73.17481
333 [9] Vijayakumar M, Parammasivam KM, Rajagopal S (2024) Effect of torrential rainfall on aerodynamic characteristics of
334 MALE UAV with two element airfoil wing using CFD approach. Defence Science Journal 74:804-811. https://doi.org/10.1
335 4429/dsj.74.19904
336 [10] Wu Z, Lv B, Cao Y (2018) Heavy rain effects on aircraft lateral/directional stability and control determined from num
337 erical simulation data. Aerospace Science and Technology 80:472-481. https://doi.org/10.1016/j.ast.2018.07.037
338 [11] Zhang RM, Cao YH (2011) Study of the mechanisms underlying the effects of rainfall on airfoil aerodynamic perform
339 ance. Flight Dynamics 29:70-73
340 [12] Yuan PJ, Chang SJ, Dai YW et al (2024) Numerical calculation of the aerodynamic characteristics of low-speed aircra
341 ft under heavy rain conditions. Aero Weaponry 31:127-135. https://doi.org/10.12132/ISSN.1673-5048.2024.0133
342 [13] Yang P, Chang SJ, Zhang JW (2022) Numerical simulation of the aerodynamic characteristics of a projectile in a heav
343 y rain environment. Journal of Ballistics 34:33-40. https://doi.org/10.12115/j.issn.1004-499X(2022)02-005
344 [14] Wu Z, Cao Y, Ismail M (2013) Numerical simulation of airfoil aerodynamic penalties and mechanisms in heavy rain. I
345 nternational Journal of Aerospace Engineering 2013:1-13. https://doi.org/10.1155/2013/590924
346 [15] Markowitz AH (1976) Raindrop size distribution expressions. Journal of Applied Meteorology 15:1029-1031
347 [16] Ismail M, Cao YH, Wu ZL et al (2014) Numerical study of aerodynamic efficiency of a wing in simulated rain environ
348 ment. Journal of Aircraft 51:2015-2023. https://doi.org/10.2514/1.C032557